Phonon Density of States of Single-Wall Carbon Nanotubes

S. Rols,[1,2] Z. Benes,[3] E. Anglaret,[1] J. L. Sauvajol,[1] P. Papanek,[3,4] J. E. Fischer,[3] G. Coddens,[5]
H. Schober,[2] and A. J. Dianoux[2]

[1]*Groupe de Dynamique des Phases Condensées (UMR CNRS 5581), Université Montpellier II, 34095 Montpellier Cedex 5, France*
[2]*Institut Laue-Langevin, 38042 Grenoble Cedex, France*
[3]*Department of Materials Science and Engineering and Laboratory for Research on the Structure of Matter, University of Pennsylvania, Philadelphia, Pennsylvania 19104*
[4]*Center for Neutron Research, National Institute of Standards and Technology, Gaithersburg, Maryland 20899*
[5]*Laboratoire Léon Brillouin (CEA/CNRS), CE Saclay, 91191 Gif-sur-Yvette Cedex, France*
(Received 1 March 2000)

The vibrational density of states of single-wall carbon nanotubes (SWNT) was obtained from inelastic neutron scattering data from 0 to 225 meV. The spectrum is similar to that of graphite above 40 meV, while intratube features are clearly observed at 22 and 36 meV. An unusual energy dependence below 10 meV is assigned to contributions from intertube modes in the 2D triangular lattice of SWNT bundles, and from intertube coupling to intratube excitations. Good agreement between experiment and a calculated density of states for the SWNT lattice is found over the entire energy range.

PACS numbers: 78.70.Nx, 61.46.+w, 61.48.+c

Single-wall carbon nanotubes (SWNT) are promising systems both for applications and basic science in one dimension [1]. Many of their physical properties, especially mechanical and transport, are known to depend on molecular structure (diameter, chirality), bundlelike crystalline packing [2], and corresponding lattice dynamics. Despite a large number of spectroscopic studies, the experimental information has been so far limited to $Q = 0$ Raman-active [3] and infrared-active modes [4]. Most of the numerical investigations [dispersion curves, vibrational density of states (VDOS)] treated mainly isolated SWNT [1,5]. Therefore little is known about low-energy intratube (bends and twists), and intertube excitations (librations, acoustic phonons) within the bundles, neither of which are easily accessible by optical techniques. It is these low-energy excitations that are believed to play an important role in the temperature dependence of the electronic conductivity [6] and the low T heat capacity [7]. Kane and Mele suggested that the temperature dependence of the electronic conductivity arises from low frequency *electron-phonon coupling,* in particular the low-frequency intratube twist mode (expected between 1 and 5 meV) which is an efficient backscattering mechanism for conduction electrons [6]. Recently, Mizel *et al.* measured Cp of SWNT and attempted to explain its peculiar low T behavior in terms of VDOS model calculations for individual SWNT and a SWNT crystal; neither agreed with their data very well [7].

Consequently, experimental and numerical studies of the low-frequency dynamics of bundles and single tubes, including nonzero wave-vector contributions, are required. Here we present the first VDOS measurement for any carbon nanotube material, using inelastic neutron scattering (INS) over a large phonon energy range 0–225 meV, using 3 different instruments to cover this range with good overlap of the data. We analyze and discuss the results with the aid of calculations which account for lattice effects in bundles.

When perfoming INS experiments on SWNT, sample characterization is very important for two major reasons: (a) carbon is a weak scatterer of neutrons so impurity effects must be minimized; and (b) the measured VDOS is expected to be very sensitive to crystallinity at low energy. Nickel is a typical catalyst, and some strong Ni modes overlap with SWNT radial breathing modes (15–40 meV). Similarly, the VDOS of graphitic impurities will overlap with the SWNT contribution, especially at high energies. Finally, hydrogen has a very large incoherent cross section such that even a small amount can severely modify the measured VDOS. While hydrogen is not normally a contaminant in nanotubes, the large surface area suggests the possibility of adsorbed water from handling/storing in air.

Our nanotube sample was prepared by pulsed laser vaporization using 0.6 at. % each Co and Ni catalysts well dispersed in the graphite target [8]. Acid purification and microfiltration removed most of the residual metals, amorphous carbon, and graphitic impurities. The final water suspension with surfactant was centrifuged to dryness, then vacuum annealed at 1200 °C for 1 h to improve the crystallinity [8] and remove all traces of surfactant. To avoid traces of water, the sample was vacuum dried for 24 h at 200 °C prior to each neutron experiment. We also measured a graphite standard for comparison with the SWNT.

Characterization was performed by high resolution transmission electron microscopy (HRTEM), x-ray and neutron diffraction, which probe mass scales of $\sim$ fg, $\sim$ mg, and our entire 540 mg sample, respectively. HRTEM showed a prevalence of bundles over isolated tubes, with very little encapsulated C_{60}, onions, or graphitelike nanoshells [9]. X-ray diffraction was in good agreement with previous results on similar material [8]. The most stringent test of diameter uniformity and overall

 0031-9007/00/85(24)/5222(4)$15.00

homogeneity is obtained from neutron diffraction on the entire sample. This was done using the multidetector powder diffractometers BT-1 at the National Institute of Standards and Technology (NIST) and G4-1 at the Laboratoire Léon Brillouin (LLB), which gave essentially identical results. The room temperature G4-1 profile is shown in Fig 1. The peak at 1.87 $Å^{-1}$ indicates the presence of a small amount of residual graphite. A much broader peak is observed at 1.82 $Å^{-1}$. From its shape and position, and in agreement with previous assigments [2], it indicates the presence of a small amount of graphitic nanoparticles. Multiwall tubes [10], onions, and nanoshells also contribute in this range. By contrast, there are almost no crystalline Ni particles in the sample, as indicated by the very weak intensity of the sharp Ni peaks at 3.1 (111) and 3.6 $Å^{-1}$ (200). Prompt gamma activation analysis of the entire sample gave total Ni and Co concentrations $\leq$0.5 at. %. The peaks at 0.45, 0.74, 1.19, and 1.66 $Å^{-1}$ are ($hk0$) signatures of the bundlelike packing of SWNT [2,8,11], while the broad asymmetric structure beginning at 2.9 $Å^{-1}$ is characteristic of intertube reflections [10]. The general agreement of our neutron data with x-ray profiles confirms the quality and *large-scale* homogeneity of our sample. Indeed several large samples prepared by laser vaporization and arc discharge by different groups were evaluated on BT-1, and the present sample exhibited the strongest intensity from the bundle lattice, as well as the weakest intensities from graphite and Ni crystallites.

We analyzed the data in Fig. 1 using a two-step process. First the profile was fit to 8 Lorentzians up to $Q = 2.5$ $Å^{-1}$, 4 of which represent small-angle scattering (centered at $Q = 0$), onions, graphite, and amorphous carbon. These 4 were then subtracted from the data, and the difference was fit to a rope lattice model which accounts for diameter dispersivity [11], shown in the inset. Good agreement was found for a mean tube diameter of 1.4 nm and a standard deviation of 0.2 nm. The number of tubes per bundle (which defines the intertube coherence length) was fixed at 40; with 7% diameter dispersivity, coherence length effects are unimportant once the number of tubes per ropes exceeds 20.

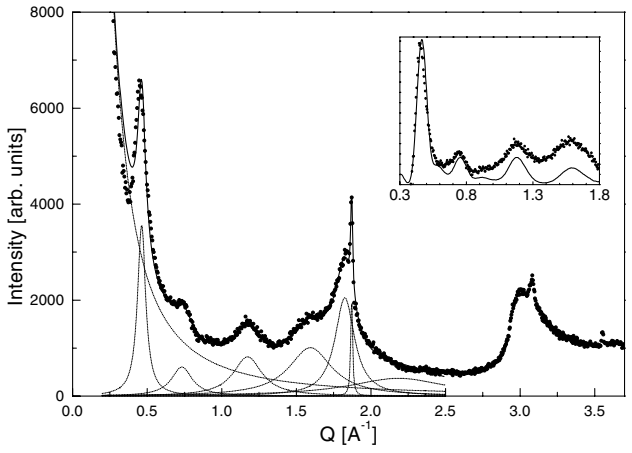

FIG. 1. Neutron diffraction spectrum of the SWNT sample, fitted to the sum of eight Lorentzians (see text for details). The inset shows a comparison between the (background + impurity)-subtracted diffraction profile and a lattice model calculation (solid line).

Inelastic neutron experiments were done using two complementary techniques. In the energy range 20–250 meV, INS investigations were performed with Be filter-analyzer spectrometers (FAS): BT-4 (thermal source) at NIST [12] and IN1B (hot source) at the Institut Laue-Langevin (ILL) [13]. In this technique, scattered neutrons are detected in an energy window defined by the Bragg cutoff of the Be (or Be + graphite) filter. These windows, 0–5 meV and 0–2 meV, respectively, set the lower bound on the energy resolution. Tuning the energy transfer from the neutron to the sample (up scattering) is achieved by scanning the incident neutron energy with a crystal monochromator (graphite or Cu).

Energies below 20 meV are accessible by cold neutron time-of-flight (TOF) spectrometry (beam line IN6 at ILL). In TOF, energy transfer occurs from the sample to the neutrons (down scattering) and the incident energy is fixed by the combination of a graphite crystal and a disk chopper [13]. The scattered neutron velocity is deduced from its monochromator-to-detector flight time. Since phonons must be present to down scatter the neutrons, TOF has to be carried out at relatively high temperature ($\geq$100 K).

In both FAS and TOF, the number of scattered neutrons is measured as a function of energy transfer. After classic data treatment [14], transformation from time to energy for TOF [13] and data analysis [14], one obtains the generalized density of states (GDOS). For coherent scatterers such as carbon, this is achieved within the framework of the "incoherent approximation" [15]. The GDOS is a well-defined function and offers a concise way of presenting the experimental data. However, one should ensure that preferred orientation does not bias the spectra. This has been ruled out by performing consistency checks between several runs. Note that in FAS the incident energy is much higher than the scattered energy, so the GDOS derived from FAS is directly proportional to the scattering cross section and the data analysis is simpler [14].

The top half of Fig. 2 shows a composite inelastic scattering spectrum (counts vs energy transfer) in the range 10–225 meV where FANS provides optimum performance. Filled circles are for the 0.5 g SWNT sample; open circles were obtained from 6 g of graphite for comparison. Above 40 meV the two spectra are very similar. Maxima around 60, 75, 100, and 175 meV are observed in both SWNT and graphite, as expected from calculations [1,5]. The most significant differences are the generally larger widths and the splitting of the 60 meV structure in SWNT. In graphite, this peak originates from only two modes at the edge of the Brillouin zone: the lowest energy acoustic out-of-plane mode, and the optical branch which is labeled B_{1g} at the zone center. By contrast, SWNT have several optic branches (analogous to 1D subbands in the electron band structure) which lead to broadening

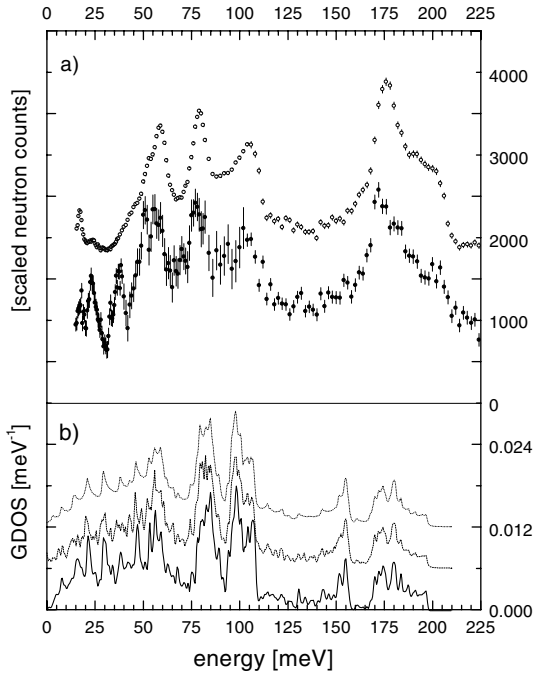

FIG. 2. (a) Inelastic neutron scattering spectra of SWNT (solid circles) and graphite (open circles) measured on filter-analyzer spectrometers BT-4 at NIST (thermal source) with graphite (15–39 meV) and Cu (39–102 meV) monochromators at 12 K; and IN1B at ILL (hot source, 102–225 meV) at 5 K. Graphite data are offset by 2000 counts for clarity. (b) Calculated phonon density of states, modulated by the amplitudes of vibrations. From top to bottom: isolated (10,10) SWNT, distribution of isolated tubes with different diameters (average diameter 1.4 nm and distribution width 0.2 nm), bundle of (10,10) SWNT.

and splitting of this peak in the GDOS. In the lower half of Fig. 2 we show calculated GDOS for various structure models: isolated (10,10) tubes (top), isolated tubes with diameter dispersion (middle), and a crystal of (10,10) tubes (bottom). For isolated tubes we used a force-constant model similar to Saito *et al.* [5]. To account for van der Waals intertube interactions we added a Lennard-Jones potential, $U(R) = 4\epsilon[(\sigma/R)^{12} - (\sigma/R)^6]$ [16] with parameters $\epsilon = 2.964$ meV and $\sigma = 3.407$ Å, given by Lu and Wang [17]. These provide the best fits to the interlayer distance and C_{33} of graphite, and also reproduce the bulk properties of solid C_{60} [17]. We included a large number of points in the first Brillouin zone, and the GDOS have been modulated by the vibration amplitudes to be closer to the experimental conditions [13,18].

From 40 to 225 meV we find generally good agreement between experiment and model calculations. In particular, the positions of features around 60, 75, 100, and 175 meV are well reproduced. By contrast, the relative intensities of the high energy bands (175 meV) are not well reproduced, and the peak at 155 meV which is predicted by all the tube models (and most graphite models) is not observed in tubes or in graphite. These discrepancies in intensities might be due to multiphonon scattering and/or anharmonicity, both of which become important at high energy. For the SWNT, all three models work equally well since the effects of diameter distribution and intertube coupling are weak in this energy range.

A key result of this paper is that SWNT and graphite spectra are significantly different in the 15–40 meV range. The SWNT sample exhibits two well-defined peaks at 22 and 36 meV which have no counterparts in graphite. Raman spectra from the same sample display intense peaks in the range 20–25 meV. These correspond to the A_{1g} radial breathing modes (RBM) for diameters in the range 1.2–1.5 nm, in good agreement with the present diffraction results [3]. Consequently, it is tempting to assign the corresponding GDOS features to extended-Q contributions from the same phonon branches which give rise to the RBM's at $Q = 0$. Indeed, calculations show that the relevant branches have flat dispersions only near the zone center [1,5,16], analogous to the famous 1D van Hove singularities in the electronic band structure. The multiplicity of Raman peaks, associated with tubes of different diameter [3], are not resolved in neutron spectrometry because of poorer resolution and intrinsic broadening by mode dispersion. The calculated GDOS for both isolated (10,10) tubes and a (10,10) bundle are in reasonable agreement with the data.

The lowest energies, 0–10 meV, are accessible only with TOF spectroscopy, which overlaps considerably with FAS above 10 meV. In Fig. 3(a) we compare experimental 300 K GDOS of SWNT (filled circles) and graphite (open circles) from 0 to 60 meV. As observed with FAS, Fig. 2 (top), significant additional GDOS contributions for SWNT are found in the range 15–40 meV. The 22 and 36 meV FAS features, attributed above to RBM-like excitations, are also observed in TOF but with significantly different intensities, whereas in the 12 K FAS data the intensities are about the same. The implication is that the dynamics responsible for one or both of these bands are temperature dependent, consistent with preliminary results from T-dependent TOF experiments. Further work is necessary to clarify this behavior.

In Figs. 3(b) and 3(c) we expand the 0–15 meV range of data (SWNT vs graphite) and calculations (isolated tube vs bundle), respectively. The enhanced GDOS in SWNT is clearly evident in the data. Model calculations show that this originates from both intratube [5] and intertube [16] excitations in SWNT bundles. The lowest frequency intratube optical branch (the first 1D subband) corresponds at $Q = 0$ to an E_{2g} Raman-active radial vibration at ~2.5 meV for isolated ~1.4 nm diameter tubes [5,16], stiffening to ~5 meV in bundles [16], Fig. 3(c). The theoretical peak at 8 meV is associated with the second 1D optical subband, and is not strongly affected by intertube interactions. The twist mode of an isolated tube is acoustic, whereas coupling to librations of neighboring tubes in a lattice produces an optic branch with a gap (and a GDOS peak) in the range 2–6 meV [6]. In our calculations this mode *also* contributes a weak feature to the GDOS of (10,10) tubes at 5 meV [16]. None of these predictions yield well-defined bands in the room-temperature GDOS,

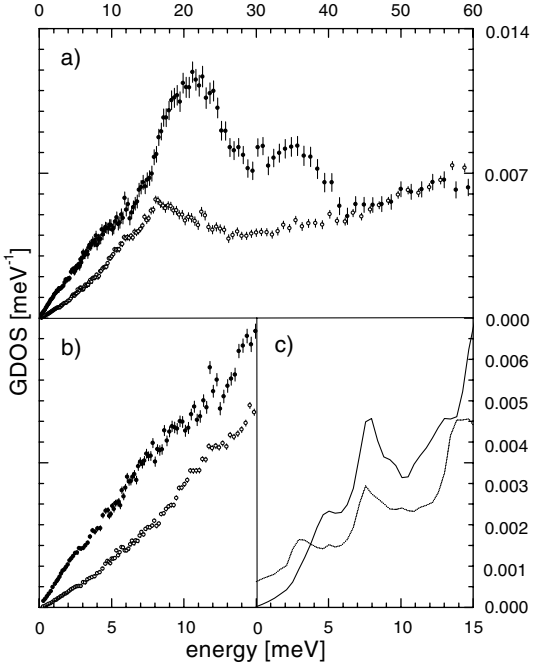

FIG. 3. (a) Room temperature GDOS of the SWNT sample (solid circles) and graphite (open circles) derived from measurements on the time-of-flight spectrometer IN6 at ILL. (b) Comparison of the low-frequency part of the SWNT and graphite data. (c) Calculated GDOS for isolated (10,10) SWNT (dotted line) and bundle of (10,10) SWNT (solid line).

Fig. 3(b). Diameter and chirality dispersion, finite bundle size, anharmonic effects, and/or disorder could broaden these modes beyond observability at 300 K. Low temperature measurements are in progress to better describe these features.

Figure 3(b) shows that the GDOS of the SWNT sample extrapolates to zero as $E \rightarrow 0$. This behavior is predicted for bundles but not for isolated tubes, Fig. 3(c), where the 1D character of an isolated tube produces a finite GDOS at $E = 0$, in disagreement with the experimental GDOS profile. We conclude that the low-frequency GDOS *in our sample* is dominated by phonons associated with the bundle lattice. This is in agreement with recent findings of Hone *et al.* [19], who measured low temperature specific heat of similar SWNT samples and showed that the acoustic phonons in the SWNT bundles are modified by intertube interactions, confirming the 3D character of SWNT bundles.

In summary, we have demonstrated the effectiveness of inelastic neutron scattering to derive the phonon density of states of nanotube samples. The GDOS is very close to that of graphite above 40 meV and significantly different below. Contributions from radial intratube modes dominate in the range 15–35 meV, while the peculiar energy dependence at very low frequencies reflects contributions from low-frequency intratube and intertube modes in the 2D triangular bundle lattice. The data suggest the possibility of a T-dependent phenomenon, perhaps analogous to molecular rotations in solid C_{60}. Good agreement is found over the entire range 0–225 meV between experiment and a model of (10,10) tubes organized into crystalline bundles.

We acknowledge Gilles André, Alexander Ivanov, and Brian Toby/Judith Stalick for their help with the neutron scattering measurements at LLB, ILL, and NIST, respectively, and are grateful to Brian Smith for the HRTEM analysis. The sample was graciously provided by M. Emrich and D. T. Colbert from Rice University. S. R. acknowledges the Région Languedoc-Roussillon for financial support. The Penn/NIST contribution was supported by the U.S. Department of Energy, DEFG02-98ER45701 (Z. B., J. E. F.) and the NSF MRSEC Program No. DMR96-32598 (PP). Travel support for the U.S./France collaboration was provided by NSF (DMR98-02560) and CNRS (PICS 611).

[1] R. Saito, G. Dresselhaus, and M. S. Dresselhaus, *Physical Properties of Carbon Nanotubes* (Imperial College Press, London, 1998).
[2] A. Thess *et al.,* Science **273**, 483 (1996).
[3] A. M. Rao *et al.,* Science **275**, 187 (1997); M. A. Pimenta *et al.,* Phys. Rev. B **58**, R16 016 (1998); L. Alvarez *et al.,* Chem. Phys. Lett. **316**, 186 (2000).
[4] E. Anglaret *et al.,* in *Electronic Properties of Novel Materials Progress in Molecular Nanostructures, Proceedings of the XIIth International Winterschool,* edited by Hans Kuzmany, AIP Conf. Proc. No. 442 (AIP, New York, 1998), p. 116; H. Kuhlmann *et al., ibid.*, p. 123.
[5] R. Saito *et al.,* Phys. Rev. B **57**, 4145 (1998).
[6] C. L. Kane *et al.,* Europhys. Lett. **41**, 683 (1998).
[7] A. Mizel *et al.,* Phys. Rev. B **60**, 3264 (1999).
[8] A. G. Rinzler *et al.,* Appl. Phys. A **67**, 29 (1998).
[9] B. W. Smith, M. Monthioux, and D. E. Luzzi, Nature (London) **396**, 323 (1998).
[10] D. Reznik, C. H. Olk, D. A. Neumann, and J. R. D. Copley, Phys. Rev. B **52**, 116 (1995).
[11] S. Rols *et al.,* Eur. Phys. J. B **10**, 263 (1999).
[12] R. R. Cavanagh, J. J. Rush, and R. D. Kelley, in *Vibrational Spectroscopy of Molecules on Surfaces,* edited by J. T. Yates and T. E. Madey (Plenum Publishing, New York, 1987), p. 183.
[13] M. Bée, *Quasielastic Neutron Scattering: Principles and Applications in Solid State Chemistry, Biology and Material Science* (Adam Hilger, Bristol, 1988).
[14] P. Papanek *et al.,* Phys. Rev. B **50**, 15 668 (1994).
[15] J. M. Carpenter and C. A. Pelizarri, Phys. Rev. B **12**, 2391 (1975); M. M. Bredov *et al.,* Sov. Phys. Solid State **9**, 214 (1967).
[16] S. Rols (unpublished).
[17] J. P. Lu and W. Yang, Phys. Rev. B **49**, 11 421 (1994).
[18] W. Marshall and S. W. Lovesey, *Theory of Thermal Neutron Scattering* (Clarendon Press, Oxford, 1971).
[19] J. Hone *et al.,* Science **289**, 1730 (2000).